Dodecatwistarene Imides with Zigzag-Twisted Conformation for Organic Electronics

Dodecatwistarene Imides with Zigzag-Twisted Conformation for Organic Electronics

Guogang Liu[a,e], Chengyi Xiao[c], Fabrizia Negri[d], Yan Li*[a,e], and Zhaohui Wang[a,b]

Abstract: 1D nonplanar graphene nanoribbons generally have three possible conformers: helical, zigzag, and mixed conformations. In this research, a novel kind of 1D nonplanar graphene nanoribbon, namely dodecatwistarene imides featuring twelve linearly fused benzene rings, was obtained by bottom-up synthesis of palladium-catalyzed Stille coupling and C-H activation. Single-crystal X-ray diffraction analyses revealed that it displays a zigzag-twisted conformation caused by steric hindrance between imide groups and neighbouring annulated benzene rings with the pendulum angle of 53°. This conformation is very stable and could not convert to other conformations even when heated up to 250 ºC for 6 hours. Despite of the highly twisted topology, organic field-effect transistor based on it exhibits electron mobility up to 1.5 $cm^2 V^{-1} s^{-1}$ after annealing.

In recent years, the diverse topology of nanographenes with large nonplanar π-systems has invigorated the synthesis of multi-dimensional nonplanar polycyclic aromatic hydrocarbons.[1-3] Among them, one-dimensional (1D) nonplanar graphene nanoribbons, such as twistacenes and twistarenes containing long linearly fused benzene rings, have attracted much attention on account of their extraordinary optical and electronic properties, and packing modes derived from their unique topology.[4,5] In general, 1D nonplanar graphene nanoribbons have three possible conformers: helical, zigzag, and mixed conformations, caused by the steric-hindrance effect of introducing substituents on the periphery of conjugated backbones.[6] The strategy of introducing imide groups is recently considered as an effective method to not only improve the stability and solubility of nonplanar nanographenes, but also modulate their energy levels and charge-transport abilities.[7]

Until now, twistacenes and twistarenes with helical conformation have been reported by us and others.[8] For example, a decatwistacene imides featuring ten linearly fused benzene rings was reported by us recently via palladium-catalyzed Suzuki cross-coupling and C-H activation.[8a] Single-crystal structure of it exhibits a helical conformation as shown in Figure 1a, which has potential application in chiroptical devices. However, the design and synthesis of 1D nonplanar graphene nanoribbons with zigzag-twisted conformation and their applications in organic electronics are rarely reported. Herein, we designed and synthesized a novel kind of 1D nonplanar graphene nanoribbons, namely dodecatwistarene imides featuring twelve linearly fused benzene rings as shown in Figure 1b. In contrast to the helical conformation of decatwistacene imides, dodecatwistarene imides displays a zigzag conformation with the pendulum angle of 53°. Despite of the highly twisted topology, organic field-effect transistors based on it exhibit electron mobility up to 1.5 $cm^2 V^{-1} s^{-1}$ under ambient conditions.

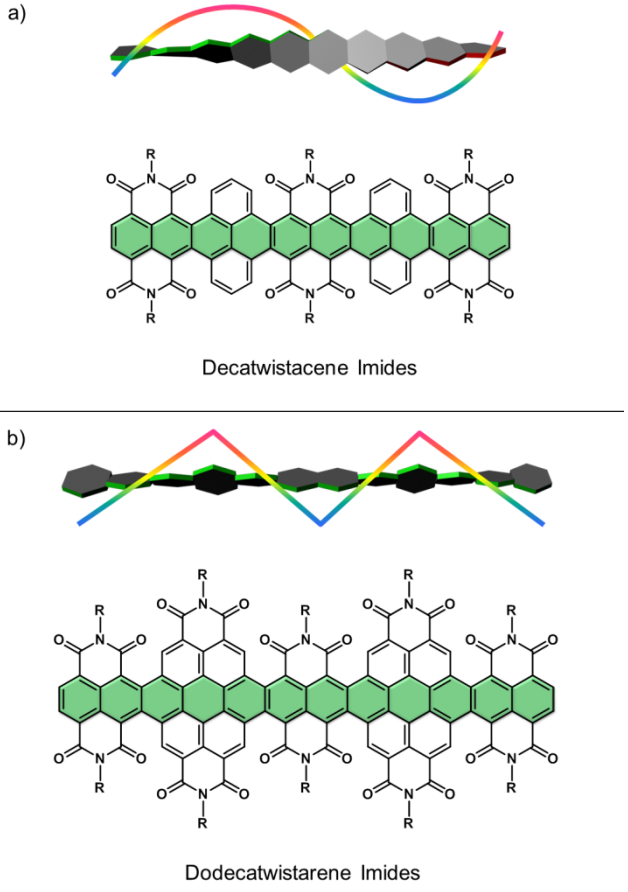

Figure 1. Two topology of 1D nonplanar graphene nanoribbons. a) Molecular structure of decatwistacene imides featuring helical conformation and b) molecular structure of dodecatwistarene imides featuring zigzag conformation.

Scheme 1 illustrates the synthesis of dodecatwistarene imides. Monostannyl-naphthalene diimides (NDI) **1** and distannyl-NDI **4** were obtained according to a known procedure.[9] The key precursor compound **3** retaining two chlorine atoms in the bay region of PDI subunit was obtained in 60% yield under the $Pd(PPh_3)_4$/CuI system with the ratio of starting materials monostannyl-NDI **1** and tetrachlorinated PDI **2** about 1:1. When compound **3** was used subsequently as a building block to react

[a] G. Liu, Prof. Y. Li, Prof. Z. Wang
Key Laboratory of Organic Solids
Institute of Chemistry, Chinese Academy of Sciences
Beijing 100190, China
E-mail: yanli@iccas.ac.cn
[b] Prof. Z. Wang
Key Laboratory of Organic Optoelectronics and Molecular Engineering, Department of Chemistry, Tsinghua University
Beijing 100084, China
[c] C. Xiao
State Key Laboratory of Organic-Inorganic Composites, Beijing University of Chemical Technology
Beijing 100029, China
[d] Prof. F. Negri
Dipartimento di Chimica "G. Ciamician", Università di Bologna, Via F. Selmi, 2, 40126 Bologna, Italy
[e] G. Liu, Prof. Y. Li
School of Chemistry and Chemical Engineering, University of Chinese Academy of Sciences
Beijing 100049, China

Supporting information for this article is given via a link at the end of the document.

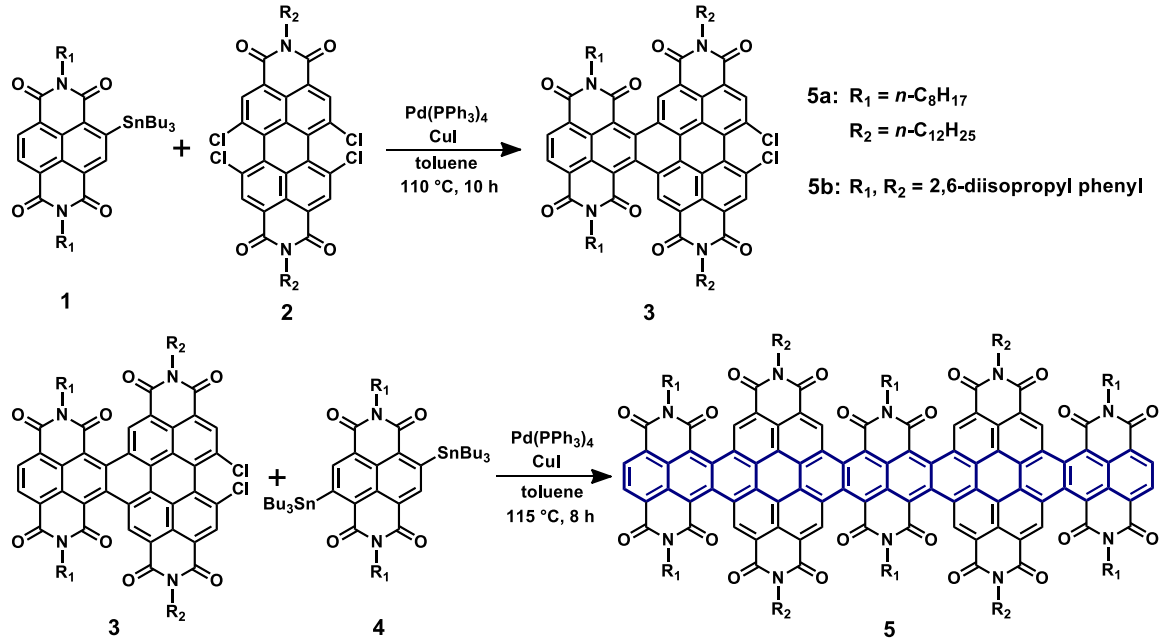

Scheme 1. Synthetic route to dodecatwistarene imides **5**.

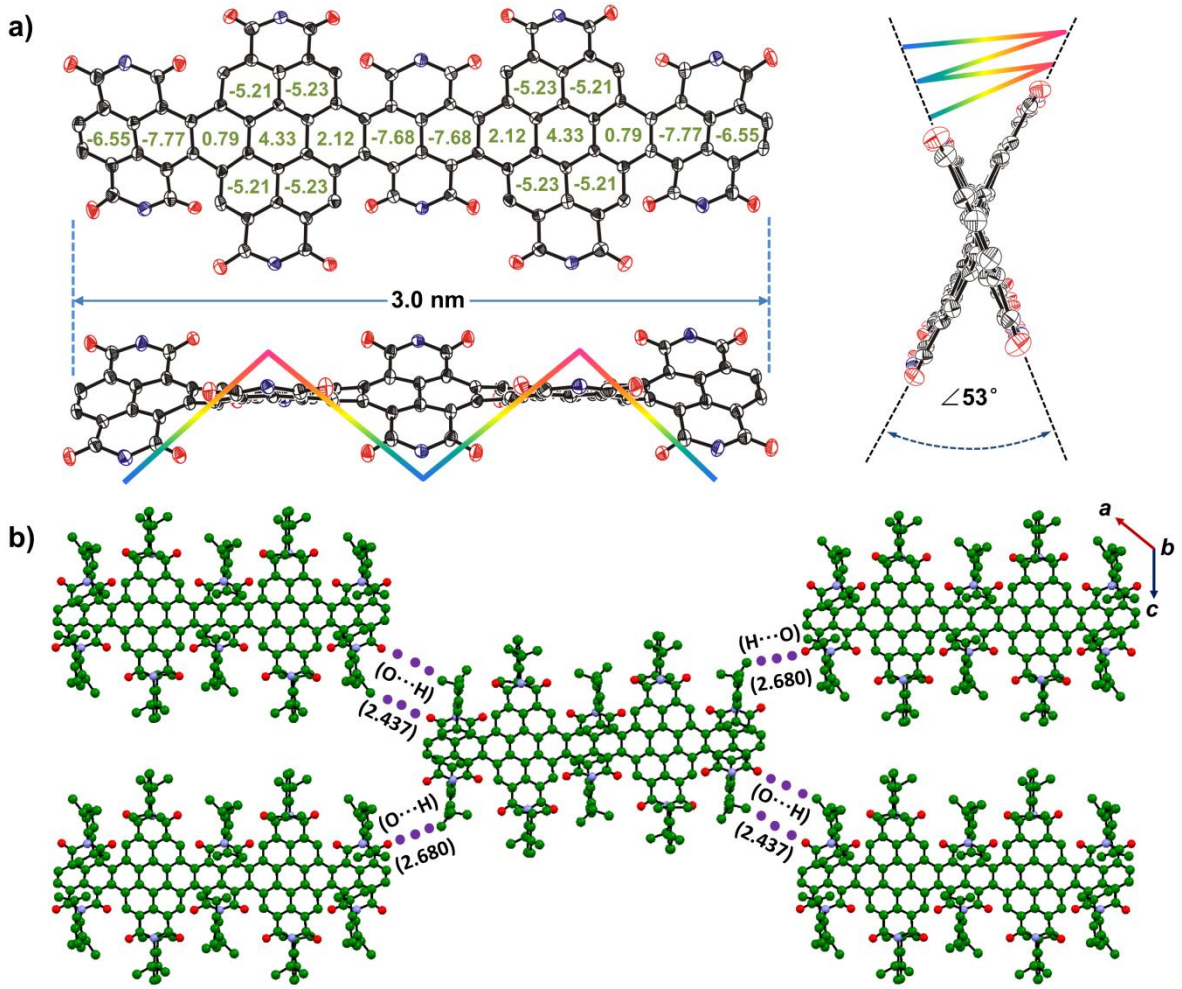

Figure 2. a) Single-crystal X-ray diffraction structure of **5b** with top and side views (ORTEP drawing at 30% probability ellipsoids) and NICS (0) values calculated at B3LYP/6-311+G** level. The diisopropyl phenyl in imide groups and hydrogen atoms are omitted for clarity. b) Crystal-packing pattern of **5b** viewed from *b* axis.

with distannyl-NDI **4** under the same condition, dodecatwistarene imides **5** was obtained in 30%~40% yields via double Stille cross-coupling and C-H activation. Interestingly, we note that the reactions between distannyl-NDI **4** and tetrachlorinated PDI or dichlorinated PDI (two chlorine atoms in the same side of bay region)[10] are failed to construct another

precursor hexatwistacene imides **6** (Figure S1) under the $Pd(PPh_3)_4$/CuI system. To investigate the topology and application of dodecatwistarene imides, two different substituents were selected: 2,6-diisopropyl phenyl groups and straight alkyl chains. Dodecatwistarene imides **5** and the precursor compound **3** were fully characterized by ^1H NMR, ^{13}C NMR, and high-resolution mass spectrometry. The thermal properties were evaluated by thermal gravimetric analysis (TGA) performed under nitrogen with the decomposition temperature of 5% weight loss above 400°C for **5a** and 450°C for **5b** (Figure S2). Noteworthy, dodecatwistarene imides with two different substituents have good solubility in common organic solvents, which are directly related to their nonplanar conjugated topology.

To gain insight into the molecular conformation, the single crystal of **5b** was obtained by the slow solvent vapor diffusion method ($CHCl_3$/hexane).[11] In order to clarify the skeleton, 2,6-diisopropyl phenyl in imide groups are omitted in Figure 2a and displayed in Figure 2b. Dodecatwistarene imides featuring twelve linearly fused benzene rings is 3.0 nm in length as shown in Figure 2a. Because of the steric-hindrance effect between imide groups and the neighboring annulated benzene rings, the whole conjugated skeleton of dodecatwistarene imides exhibits a zigzag-twisted conformation with the pendulum angle of 53°. This conformation is very stable and could not convert into helical or mixed conformations even when heated at 250°C in diphenyl ether for six hours (Figure S3). The energy barrier determined for a dimer model system including one NDI and one PDI unit, associated with an almost planar and highly strained transition state structure in which the carbonyl oxygen of the NDI moiety and the perylene hydrogen experience a huge steric repulsion, is as large as 61 kcal mol^{-1} (Figure S4). The bond lengths of C4-C5 in benzene rings 3 and 10 and C13-C19 in benzene rings 5 and 8 are 1.506 and 1.505 Å, respectively, which are much longer than other bond lengths of benzene rings owing to the large steric repulsion between NDI and PDI moiety and more closer to the $C(sp^3)$–$C(sp^3)$ bond length (Figure S5). The torsion angles α and β in rings 3 and 10 are 20.28° and 18.38°, respectively, and those in rings 5 and 8 are 21.22° and 18.27°, respectively (Figure S5). The crystal-packing pattern of **5b** along the *b*-axis and the *a*- and *c*-axis are shown in Figure 2b and Figure S6, respectively. Unlike pyrene-containing dodecatwistarene showing a perpendicular packing model between two neighboring molecules,[5c] dodecatwistarene imides exhibit a parallel packing model among the whole molecules in the crystal lattice, which is very similar to that of decatwistacene imides with helical conformation. Moreover, there are multiple C–H···O interactions between the carbonyl oxygen and 2,6-diisopropyl phenyl groups of neighboring molecules, which will facilitate the intermolecular charge transport.

The nuclear independent chemical shifts (NICS) calculation was conducted at B3LYP/6-311+G** level to provide an impression of the aromatic character of dodecatwistarene imides.

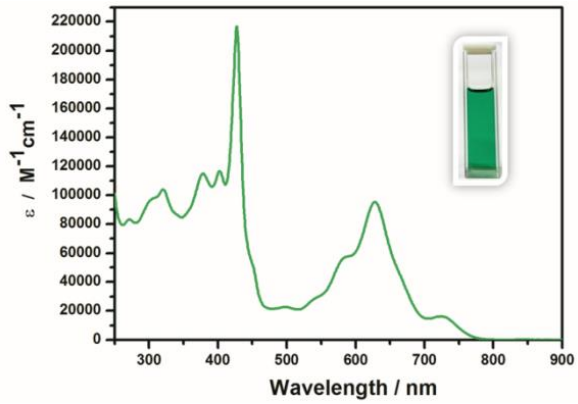

Figure 3. UV/Vis absorption spectrum of **5a** in $CHCl_3$ at room temperature (1×10^{-5} M).

As shown in Figure 2a and Figure S5, among the twelve linearly fused benzene rings, the benzene rings 1, 2, 6, 7 in NDI subunits show aromatic character, whereas the benzene rings 3, 4, 5, 8, 9, 10 in PDI subunits exhibit antiaromatic feature (0.79 ppm for rings 3 and 10, 4.33 ppm for rings 4 and 9, 2.12 ppm for rings 5 and 8). Meanwhile, the other four annulated benzene rings in perylene moiety exhibit aromatic feature (–5.21 and –5.23 ppm). This phenomenon is very similar to that of decatwistacene imides which can be considered as a combination of NDI and pyrene subunits.[8a]

The optical and electronic properties were investigated by UV/Vis absorption and fluorescence spectroscopy, and cyclic voltammetry. As shown in Figure 3 and Figure S7, **5a** and **5b** have almost the same shape and absorbance in chloroform in the visible region despite of their different substituents in imide groups. Both of them have two major absorption regions of 250–470 nm (region 1) and 470–800 nm (region 2), which is very similar to decatwistacene imides with two major absorption regions of 250–420 nm and 420–700 nm.[8a] However, dodecatwistarene imides have much higher molar extinction coefficient ($\varepsilon_{max} = 2.2 \times 10^5$ L mol^{-1} cm^{-1} for region 1, $\varepsilon_{max} = 1.0 \times 10^5$ L mol^{-1} cm^{-1} for region 2) in the whole UV/Vis region than decatwistacene imides. The lowest-energy maxima of **5a** and **5b** were at 727 nm, bathochromically shifted by 93 nm in comparison with decatwistacene imides. It was found that both compounds have weak fluorescence with the maxima at 755 nm for **5a** and 762 nm for **5b** as shown in Figure S8. Cyclic voltammogram of **5a** is shown in Figure S9. There are six obvious reversible reduction waves in CH_2Cl_2 with the half-wave reduction potentials at –0.32 V, –0.45 V, –0.65 V, –0.78 V, –0.88 V, and –1.20 V vs Fc/Fc^+, respectively, indicating that dodecatwistarene imides has strong ability to accept multiple electrons attributing to the introduction of ten imide groups to the dodecatwistarene backbone. The LUMO level of **5a** estimated from the reduction onset is –4.67 eV, much lower than that (–4.27 eV) of decatwistacene imides. The energy gap E_g obtained from the edge of the absorption spectrum in $CHCl_3$ is 1.61 eV. Thus the HOMO level calculated according to $E_{HOMO}=(E_{LUMO}-E_g)$ is –6.28 eV. The strong ability of accepting multiple electrons and low-lying LUMO level of dodecatwistarene imides will definitely facilitate the electron injection and transmission in organic electronics.

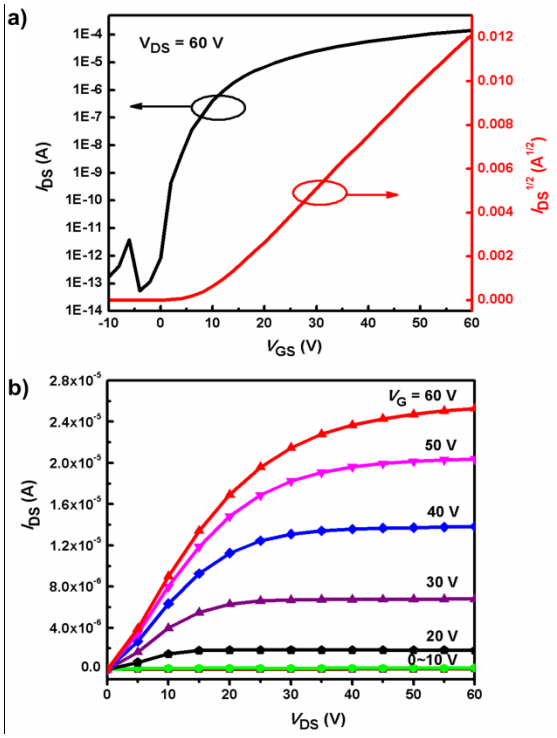

Figure 4. a) Transfer and b) output characteristics of thin film OFETs based on dodecatwistarene imides **5a**.

To explore the application in organic electronics, organic field-effect transistors based on the film of dodecatwistarene imides were fabricated. Thin films (20–40 nm in thickness) of **5a** were spin-coated from $CHCl_3$ solution on octadecyltrichlorosilane (OTS)-treated SiO_2/Si substrates. Then, thin films were annealed at 180, 200, or 220°C. Au source/drain electrodes with width/length of 200 μm/25 μm were deposited on the organic layer through a shadow mask, affording a bottom-gate top-contact device configuration. All devices were tested under ambient conditions. The unannealed thin film devices showed a moderate electron mobility of 0.26 $cm^2\ V^{-1}\ s^{-1}$. Thermal annealing of the thin films gave rise to a substantial improvement in device performance. The highest electron mobility of 1.5 $cm^2\ V^{-1}\ s^{-1}$ was achieved after annealing at 200°C accompanied with a high current on/off ratio of 8.3×10^8 and a threshold voltage of 9.28 V as shown in Figure 4, and the average electron mobility is also up to 1.3 $cm^2\ V^{-1}\ s^{-1}$ (Table S2). Atomic force microscopy (AFM) images (Figure S10) revealed that the thin film has an increased grain size and decreased grain boundaries after annealing, which are account for the high performance.

In summary, dodecatwistarene imides featuring twelve linearly fused benzene rings were synthesized in moderate yields via double Stille cross-coupling and C-H activation and were fully characterized. Single-crystal X-ray diffraction analyses revealed that unlike decatwistacene imides with helical conformation, dodecatwistarene imides displays a zigzag-twisted conformation with the pendulum angle of 53°. This conformation is very stable and no inversion was observed even at 250 ºC. The result of thin film organic field-effect transistors based on it indicates that 1D nonplanar graphene nanoribbon with zigzag conformation has wide applications in organic electronics.

Acknowledgements

This work was financially supported by the National Natural Science Foundation of China (NSFC) (No. 21672221, 21790361), the National Key R&D Program of China (2017YFA0204700), and the Youth Innovation Promotion Association of Chinese Academy of Sciences.

Conflict of interest

The authors declare no conflict of interest.

Keywords: decatwistacene imides • zigzag-twisted conformation • X-ray diffraction • optoelectronic properties • organic field-effect transistors

[1] a) A. Narita, X.-Y. Wang, X. Feng, K. Müllen, *Chem. Soc. Rev.* **2015**, *44*, 6616-6643; b) M. Ball, Y. Zhong, Y. Wu, C. Schenck, F. Ng, M. Steigerwald, S. Xiao, C. Nuckolls, *Acc. Chem. Res.* **2015**, *48*, 267-276; c) S. H. Pun, Q. Miao, *Acc. Chem. Res.* **2018**, *51*, 1630-1642.

[2] a) K. Shoyama, F. Würthner, *J. Am. Chem. Soc.* **2019**, *141*, 13008-13012; b) K. Kawasumi, Q. Zhang, Y. Segawa, L. T. Scott, K. Itami, *Nat. Chem.* **2013**, *5*, 739-744; c) K. Y. Cheung, C. K. Chan, Z. Liu, Q. Miao, *Angew. Chem. Int. Ed.* **2017**, *56*, 9003-9007; *Angew. Chem.* **2017**, *129*, 9131-9135; d) L. T. Scott, E. A. Jackson, Q. Zhang, B. D. Steinberg, M. Bancu, B. Li, *J. Am. Chem. Soc.* **2012**, *134*, 107-110; e) K. Xu, J. I. Urgel, K. Eimre, M. Di Giovannantonio, A. Keerthi, H. Komber, S. Wang, A. Narita, R. Berger, P. Ruffieux, C. A. Pignedoli, J. Liu, K. Müllen, R. Fasel, X. Feng, *J. Am. Chem. Soc.* **2019**, *141*, 7726-7730.

[3] a) Y. Hu, X.-Y. Wang, P.-X. Peng, X.-C. Wang, X.-Y. Cao, X. Feng, K. Müllen, A. Narita, *Angew. Chem. Int. Ed.* **2017**, *56*, 3374-3378; *Angew. Chem.* **2017**, *129*, 3423-3427; b) G. Liu, T. Koch, Y. Li, N. L. Doltsinis, Z. Wang, *Angew. Chem. Int. Ed.* **2019**, *58*, 178-183; *Angew. Chem.* **2019**, *131*, 184-189; c) D. Meng, G. Liu, C. Xiao, Y. Shi, L. Zhang, L. Jiang, K. K. Baldridge, Y. Li, J. S. Siegel, Z. Wang, *J. Am. Chem. Soc.* **2019**, *141*, 5402-5408; d) N. J. Schuster, R. H. Sánchez, D. Bukharina, N. A. Kotov, N. Berova, F. Ng, M. L. Steigerwald, C. Nuckolls, *J. Am. Chem. Soc.* **2018**, *140*, 6235-6239; e) Y. Zhu, X. Guo, Y. Li, J. Wang, *J. Am. Chem. Soc.* **2019**, *141*, 5511-5517.

[4] a) R. A. Pascal, Jr., *Chem. Rev.* **2006**, *106*, 4809-4819; b) M. Rickhaus, M. Mayor, M. Juríček, *Chem. Soc. Rev.* **2016**, *45*, 1542-1556.

[5] a) Y. Zhong, T. J. Sisto, B. Zhang, K. Miyata, X.-Y. Zhu, M. L. Steigerwald, F. Ng, C. Nuckolls, *J. Am. Chem. Soc.* **2017**, *139*, 5644-5647; b) Y. Zhong, M. T. Trinh, R. Chen, G. E. Purdum, P. P. Khlyabich, M. Sezen, S. Oh, H. Zhu, B. Fowler, B. Zhang, W. Wang, C.-Y. Nam, M. Y. Sfeir, C. T. Black, M. L. Steigerwald, Y.-L. Loo, F. Ng, X.-Y. Zhu, C. Nuckolls, *Nat. Commun.* **2015**, *6*, 8242; c) W. Chen, X. Li, G. Long, Y. Li, R. Ganguly, M. Zhang, N. Aratani, H. Yamada, M. Liu, Q. Zhang, *Angew. Chem. Int. Ed.* **2018**, *57*, 13555-13559; *Angew. Chem.* **2018**, *130*, 13743-13747; d) S. Ito, S. Hiroto, S. Lee, M. Son, I. Hisaki, T. Yoshida, D. Kim, N. Kobayashi, H. Shinokubo, *J. Am. Chem. Soc.* **2015**, *137*, 142-145.

[6] Y. Zhong, B. Kumar, S. Oh, M. T. Trinh, Y. Wu, K. Elbert, P. Li, X. Zhu, S. Xiao, F. Ng, M. L. Steigerwald, C. Nuckolls, *J. Am. Chem. Soc.* **2014**, *136*, 8122-8130.

[7] a) H. Xin, C. Ge, X. Jiao, X. Yang, K. Rundel, C. R. McNeill, X. Gao, *Angew. Chem. Int. Ed.* **2018**, *57*, 1322-1326; *Angew. Chem.* **2018**, *130*, 1336-1340; b) F. Zhang, Y. Hu, T. Schuettfort, C. Di, X. Gao, C. R. McNeill, L. Thomsen, S. C. B. Mannsfeld, W. Yuan, H. Sirringhaus, D. Zhu, *J. Am. Chem. Soc.* **2013**, *135*, 2338-2349; c) K. Cai, J. Xie, D. Zhang, W. Shi, Q. Yan, D. Zhao, *J. Am. Chem. Soc.* **2018**, *140*, 5764-5773; d) K. Cai, J. Xie, D. Zhao, *J. Am. Chem. Soc.* **2014**, *136*, 28-31.

[8] a) W. Fan, T. Winands, N. L. Doltsinis, Y. Li, Z. Wang, *Angew. Chem. Int. Ed.* **2017**, *56*, 15373-15377; *Angew. Chem.* **2017**, *129*, 15575-15579; b) W. Yue, J. Gao, Y. Li, W. Jiang, S. Di Motta, F. Negri, Z. Wang, *J. Am. Chem. Soc.* **2011**, *133*, 18054-18057; c) J. Lu, D. M. Ho, N. J. Vogelaar, C. M. Kraml, R. A. Pascal, Jr., *J. Am. Chem. Soc.* **2004**, *126*, 11168-11169; d) J. Lu, D. M. Ho, N. J. Vogelaar, C. M. Kraml, S.

Bernhard, N. Byrne, L. R. Kim, R. A. Pascal, Jr., *J. Am. Chem. Soc.* **2006**, *128*, 17043-17050; e) R. G. Clevenger, B. Kumar, E. M. Menuey, K. V. Kilway, *Chem. Eur. J.* **2018**, *24*, 3113-3116.

[9] L. E. Polander, A. S. Romanov, S. Barlow, D. K. Hwang, B. Kippelen, T. V. Timofeeva, S. R. Marder, *Org. Lett.* **2012**, *14*, 918-921.

[10] Y. Zhen, H. Qian, J. Xiang, J. Qu, Z. Wang, *Org. Lett.* **2009**, *11*, 3084-3087.

[11] CCDC 1940982 (**5b**) contains the supplementary crystallographic data for this paper. These data can be obtained free of charge from The Cambridge Crystallographic Data Centre via www.ccdc.cam.ac.uk/data_request/cif.